ACS APPLIED MATERIALS & INTERFACES

www.acsami.org

Research Article

Artificial Nacre Epoxy Nanomaterials Based on Janus Graphene Oxide for Thermal Management Applications

Yang Wang, Zheng Zhang, Ting Li, Piming Ma, Xuhui Zhang, Bihua Xia, Mingqing Chen, Mingliang Du, Tianxi Liu, and Weifu Dong*

Cite This: *ACS Appl. Mater. Interfaces* 2020, 12, 44273−44280

Read Online

ACCESS | Metrics & More | Article Recommendations | Supporting Information

ABSTRACT: Owing to the development of microelectronics, demands for excellent thermal dissipation materials have substantially increased. Learning from natural nacre, thermally conductive epoxy nanocomposites were prepared based on asymmetrically polydopamine-functionalized Janus graphene oxide (JPGO) scaffolds. The required highly oriented JPGO scaffolds were prepared via the bidirectional freeze-casting method. With the addition of epoxy resin, the resulting nanocomposite reveals anisotropic thermal properties. With the total content of the JPGO scaffold being 0.93 wt %, almost 35 times enhancement of in-plane thermal conductivity (perpendicular to the lamellar structure) (~5.6 W m^{-1} K^{-1}) has been obtained. The single-side-functionalized JPGO scaffolds play an important role in forming thermal conductive networks for the epoxy nanocomposites. Importantly, the nanocomposites present electrically insulating properties (>10^{14} Ω cm). Such high-performance nanocomposites have promising applications for thermal management in electronic devices.

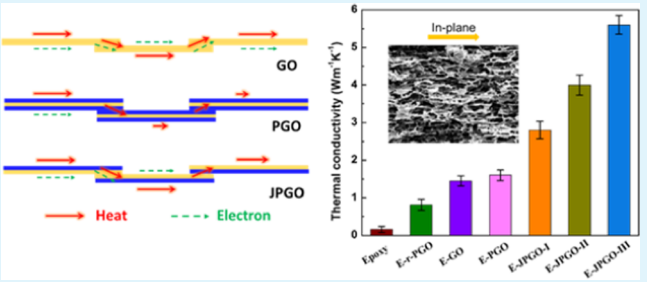

KEYWORDS: *nacre, graphene oxide, polydopamine, thermal conductivity, thermal management*

INTRODUCTION

Over the past decade, with the development of high speed and power portable electronic devices, thermally conductive but electrically insulating thermal management materials (TMMs) have been in high demand.[1−4] Polymers are electrically insulating and have been used as TMMs. However, many polymers show low thermal conductivity (0.1−0.5 W m^{-1} K^{-1}), which hinders their application in the electronic field.[5,6] A variety of nanofillers, including metal oxides and metal nitride have been employed to composite with polymers to improve the heat conductivity performance.[7−10] Nevertheless, nanocomposites with desired heat-conducting properties are usually obtained with high filler content (>50%), affecting light-weight, mechanical, or processing properties of a polymer matrix.[11,12]

Because interfacial thermal resistance is the key factor decreasing the thermal transfer efficiency, intimate interfaces and structures with well-designed orientation are effective approaches to increase thermal conductivity, as it is dependent on effective phonon transfer. The network of continuous interconnecting fillers can afford heat transport, which dramatically reduces the interfacial thermal resistance between a matrix and fillers.[13−15] For instance, Tian et al. developed a foam-templated method to design thermal conductive epoxy composites with interconnected boron nitride networks.[16] Jiang et al. fabricated a network of boron nitride nanosheets (BNNSs) via the self-assembly of BNNSs on cellulose and further with the addition of epoxy. With 9.6 vol % BNNS, high thermal conductivity (~3.1 W m^{-1} K^{-1}) of the epoxy composite was achieved.[17] Wu et al. prepared a highly thermally conductive CNF/f-BNNS film with an oriented structure by vacuum-assisted filtration.[18] Chen et al. prepared thermally conductive PVDF/BNNS composites (16.3 W m^{-1} K^{-1}) by the electrospinning process.[15] The oriented BNNS network offers a thermal conduction pathway.

In recent years, carbon materials, such as carbon nanotubes, graphene, and its derivatives, have been used to composite with polymers due to their excellent properties (thermal conductivities in the range of ~2000−5000 W m^{-1} k^{-1}).[19−21] Freeze-casting is considered as one of the suitable candidates for preparation of carbon-based materials with layer architecture, such as artificial nacre, polymer foams, and graphene aerogels.[22−24] However, carbon-based fillers always decrease the electrical insulation of polymers. To improve the thermal conductivities of polymers while maintaining excellent

Received: June 17, 2020
Accepted: September 1, 2020
Published: September 1, 2020

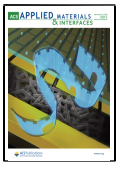

https://dx.doi.org/10.1021/acsami.0c11062
ACS Appl. Mater. Interfaces 2020, 12, 44273−44280

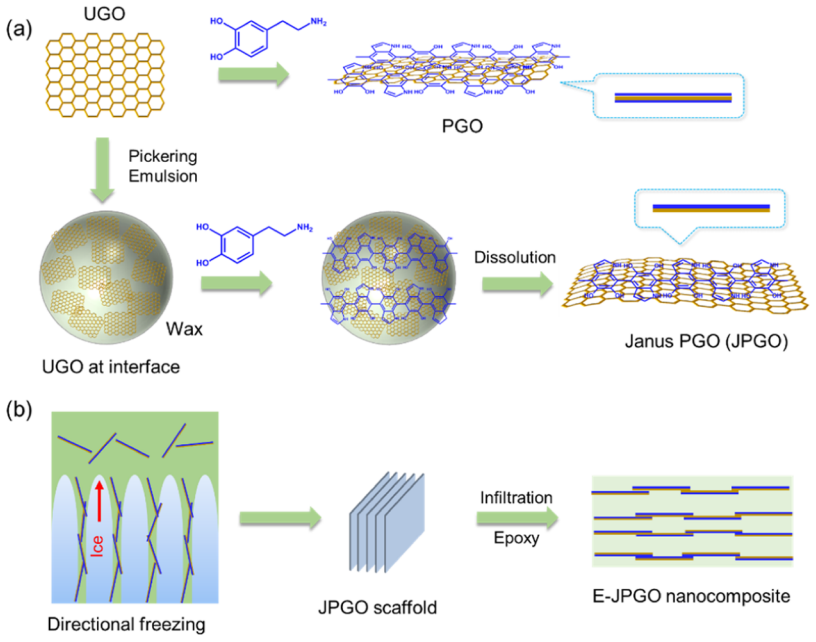

Figure 1. Schematic illustration of fabrication of (a) JPGO and (b) E-JPGO nanocomposites.

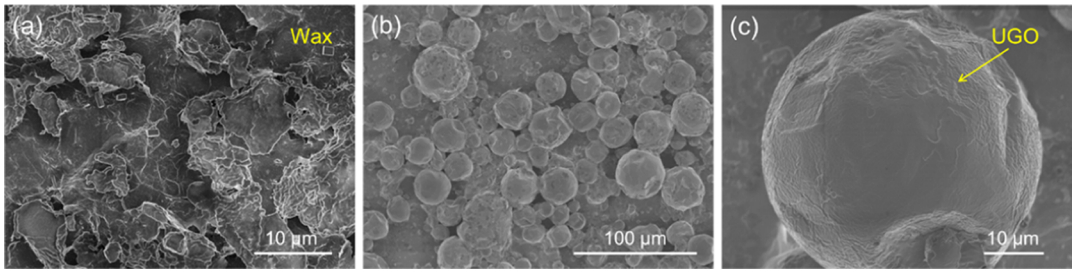

Figure 2. SEM of pure wax (a), and the stability of wax microspheres by GO (b, c) showing the wrinkled surface morphology.

insulation, various techniques have been developed to solve the crucial issue, such as the tailored distribution of the filler network and surface modification of carbon materials with insulating nanoparticles or nanolayers. To our knowledge, polydopamine (PDA) is a bioinspired material from the mussel adhesive proteins, which provides a way to the modification of various substances.[25] In our previous work, epoxy composites were fabricated with addition of PDA-coated CuNWs (copper nanowires). The PDA enhances the electric insulation properties of CuNWs. The epoxy nanocomposites own high thermally conductive and electrically insulating properties.[26]

Herein, the epoxy nanocomposites with a nacre-mimetic conductive pathway were prepared through a freeze-casting method. As shown in Figure 1, the asymmetrically polydopamine-functionalized Janus graphene oxide (JPGO) was assembled into a scaffold with a well-aligned structure, followed by addition of epoxy. JPGO scaffolds form a thermal transport channel in epoxy composites and gain high thermal conductivity at a relatively low JPGO loading. What is more, due to the polydopamine coating, the resulting nanocomposite exhibits significant potential applications for TMMs.

EXPERIMENTAL SECTION

Materials. Dopamine (98%) and tris(hydroxymethyl)-aminomethane were supplied by Aladdin. The epoxy resin from Formosa Plastics Corporation was used with the curing agent of methylcyclohexene-1,2-dicarboxylic anhydride (Aladdin).

Preparation of Graphene Oxide (GO). GO was prepared using the modified Hummers method (detailed preparation is shown in the Supporting Information).[27]

Preparation of Polydopamine-Coated GO (PGO). GO dispersion (20 mL, 5 mg mL^{-1}), dopamine (50 mg), and Tris buffer (200 mL, pH 8.5) were mixed and kept at 60 °C for 24 h. The mixture was filtered with 0.2 μm pore size filters

Preparation of Janus PGO (JPGO). Saturated sodium chloride solution (7.5 mL) and GO dispersion (100 mL, 1 mg mL^{-1}) were mixed together. Then, 10 g of wax was added and placed in a 80 °C oil bath until the wax melted, followed by emulsification with a shear emulsifier (4000 rpm). The mixture was cooled to 25 °C to form GO-covered wax spheres. The wax spheres and dopamine (0.05 g) were added into water (pH 8.5). They were allowed to react for 24 h. Janus PGO was isolated by filtration and washed with hexane to dissolve the wax. Janus PGO nanosheets were filtered followed by vacuum drying.

Fabrication of JPGO Lamellar Scaffolds. The JPGO lamellar scaffolds were created by the modified bidirectional freeze-casting of JPGO dispersion (10 mg mL^{-1}), and different freezing rates were achieved by adjusting the amount of liquid nitrogen, obtaining average freezing rates of 5, 10, and 20 μm s^{-1}. After solidification and freeze-drying in a vacuum freeze-dryer for 2 days, JPGO lamellar scaffolds were obtained.

Fabrication of Inverse Artificial Nacre Nanocomposites. The inverse artificial nacres were produced by infiltrating epoxy into JPGO lamellar scaffolds, followed by curing. The resultant E-JPGO nanocomposites were composed of about 0.77, 0.84, and 0.93 wt % JPGO. For comparison, pure epoxy, epoxy/GO (E-GO), and epoxy/PGO was also prepared using the same procedure.

https://dx.doi.org/10.1021/acsami.0c11062
ACS Appl. Mater. Interfaces 2020, 12, 44273−44280

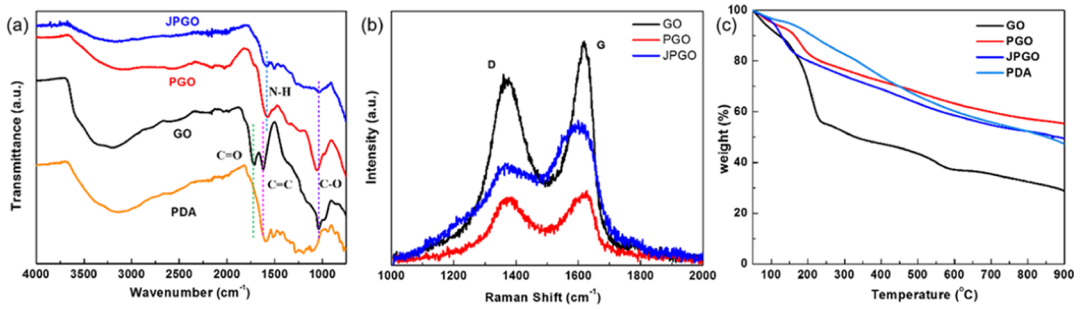

Figure 3. (a) FTIR spectra, (b) Raman spectra, and (c) thermogravimetric analysis (TGA) curves of GO, PGO, JPGO, and PDA.

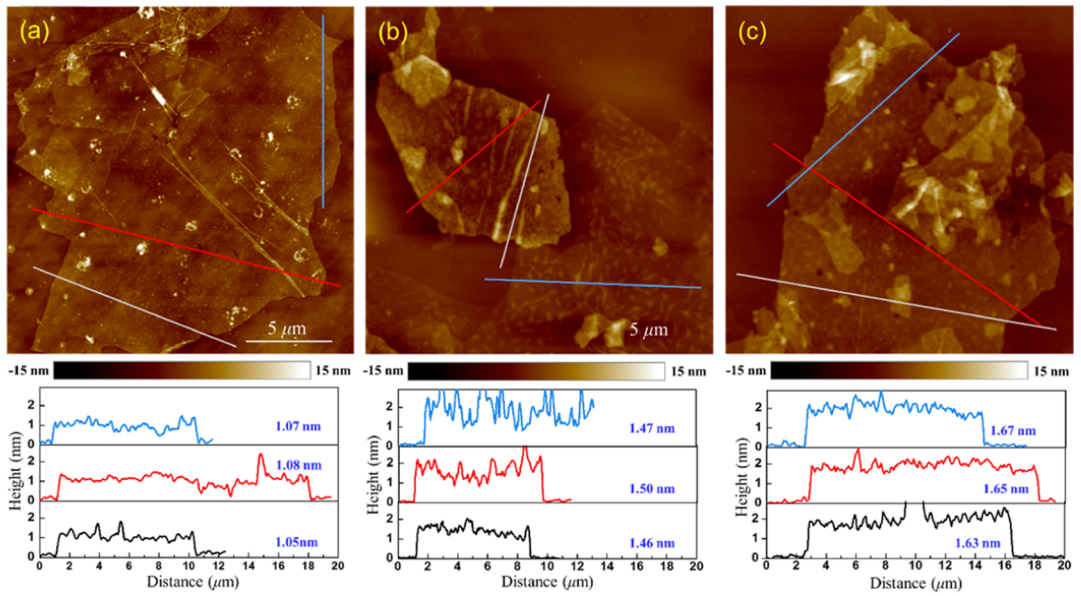

Figure 4. AFM topographic images of (a) GO, (b) JPGO, and (c) PGO, and corresponding height profiles.

Characterization. Scanning electron microscopy (SEM) investigation was conducted on a Hitachi S-4800 microscope. Fourier transform infrared (FTIR) spectra were recorded on a Nicolet 6700 spectrometer. Atomic force microscopy (AFM) was carried on Multimode 8 (Bruker) to measure the thickness of GO. The Derjaguin−Müller−Toporov (DMT) modulus images were recorded with an atomic force microscope operating in mapping mode. The thermal stability was measured by a PerkinElmer thermoanalyzer under a N_2 atmosphere. The thermal conductivity of the samples was tested by the laser flash technique (LFA 467 Hyper Flash, Netzsch). Volume resistivities were obtained on a ZC36 high resistance meter.

RESULTS AND DISCUSSION

Pickering emulsions were currently used to prepare Janus GO.[28] The wax phase was distributed on the water phase. During emulsification, amphiphilic GO was used to stabilize the emulsions. The wax microspheres were covered by wrinkled GO nanosheets (Figure 2). The wax microspheres were added into deionized water; the exposed faces of nanosheets were coated with PDA (Figure 1a).

FTIR spectra were used to detect the functional groups of GO, PGO, JPGO, and PDA. As reported in Figure 3a, the peaks of GO at 1725, 1620, and 1045 cm^{-1} are attributed to the C═O, C═C, and C−O stretching vibrations, respectively.[29] PDA has a broad peak at around 3400 cm^{-1}, which is ascribed to the aromatic −NH and −OH stretching vibrations. For PGO, the C═O stretching vibration weakens due to the GO reduction during the polymerization of PDA. A peak of PDA at 1586 cm^{-1} (N−H) is observed. No substantial differences are observed between PGO and JPGO. The structural changes in GO, PGO, and JPGO are characterized by Raman spectroscopy in Figure 3b. The peaks of D and G at ∼1370 and 1619 cm^{-1}, corresponding to the structural disorder and the graphitized structure, are observed.[30] It is interesting to note that the I_D/I_G ratio decreases upon the conversion of GO (0.833) to JPGO (0.711), suggesting a slight reduction of GO during the polymerization of PDA.[31] Typically, a higher intensity ratio (I_D/I_G) implies a larger defects level.[32] The ratio of PGO (0.929) is higher than GO, indicating increased defects and disorder structure due to the covalent PDA on the two surfaces of GO. The thermal properties of GO, PGO, and JPGO were further investigated (Figure 3c). GO exhibits a two-step degradation stage under the protection of nitrogen. The first degradation step (50−130 °C) was due to the volatilization of water. The second step of degradation (130−290 °C) relates to the oxygen-containing groups.[33] PGO and JPGO are more thermally stable than GO.

The AFM images of GO, PGO, and JPGO nanosheets are shown in Figure 4. To determine the thickness of the GO nanosheet, three different sections were chosen for the measurement. The thickness of the GO monolayer is calculated to be ∼1.07 nm. Raman spectroscopy was further used to identify the layers of GO (see Figure S1). In comparison with PGO (1.65), the thickness of JPGO is merely 1.47 nm because only one side of GO is available for coating.

https://dx.doi.org/10.1021/acsami.0c11062
ACS Appl. Mater. Interfaces 2020, 12, 44273−44280

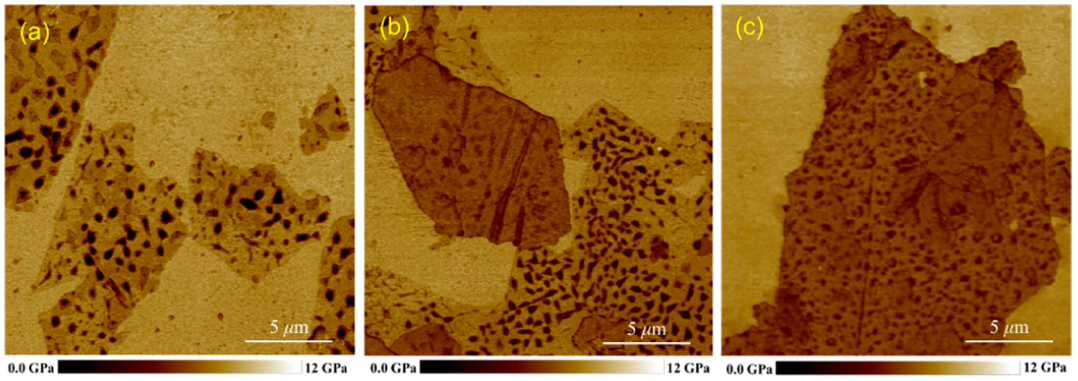

Figure 5. DMT modulus images of (a) GO, (b) JPGO, and (c) PGO.

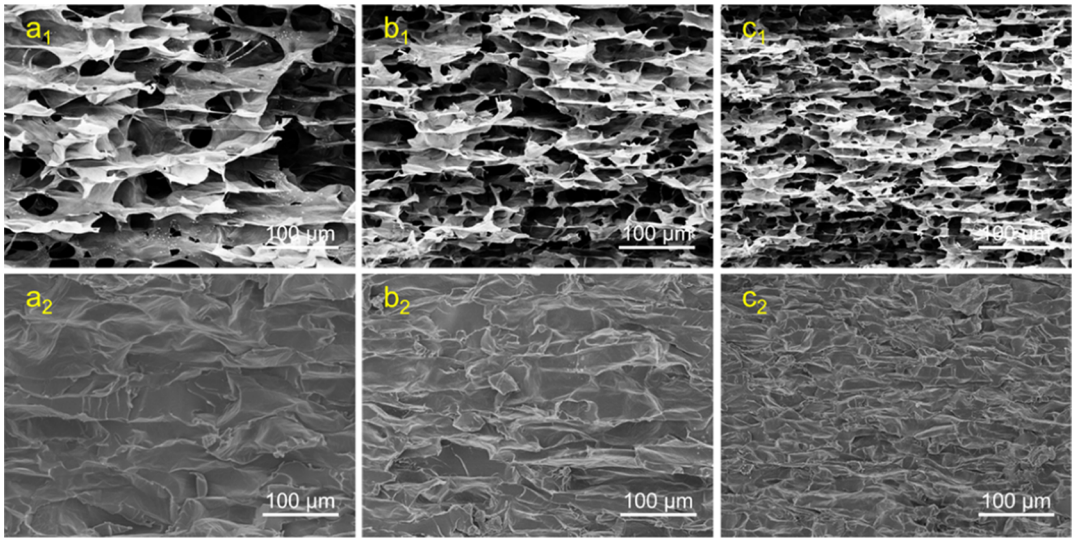

Figure 6. (a_1–c_1) Cross section images of JPGO scaffolds. (a_2–c_2) Cross section images of nacre-like E-JPGO-I, E-JPGO-II, and E-JPGO-III nanocomposites.

The DMT modulus images were recorded to observe the two faces of JPGO. As shown in Figure 5a, the light domains correspond to the high stiffness and modulus of GO.[34] PGO shows a lower modulus than GO (Figure 5c). For JPGO, two moduli were clearly detected (Figure 5b). The low modulus domains correspond to the PDA side. The high modulus domains correspond to the GO side. The DMT modulus result indicated that JPGO nanosheets were successfully prepared by the Pickering emulsion template.

The suspension of nanosheets was assembled into scaffolds through the freeze-casting method with ice as a template. The resultant JPGO scaffolds assembled with different freezing rates of $v_1 \approx 5\ \mu m\ s^{-1}$, $v_2 \approx 10\ \mu m\ s^{-1}$, and $v_3 \approx 20\ \mu m\ s^{-1}$ were named as JPGO-I, JPGO-II, and JPGO-III (Figure 6a_1–c_1), respectively. At a low freezing rate, the obtained JPGO-I scaffold shows a lamellar channel structure with a space of ~50 μm. The PGO or GO scaffold shows the same directional structure (Figure S2). Different-view morphologies of JPGO scaffolds are shown in Figure S3. The space between two adjacent sheets decreases with increasing the cooling rate. When the freezing rate was increased to $v_3 \sim 20\ \mu m\ s^{-1}$, the space between two adjacent layered walls of the JPGO-III scaffold becomes thinner (~20 μm) due to the decreasing size of ice crystals. The ice crystals endow the scaffold with aligned channels, which facilitates the penetration of liquid flow. JPGO-III was further infiltrated by epoxy to obtain the E-JPGO nanocomposite (Figure 6a_2–c_2).

For comparison, the intrinsic thermal conductivity of pure epoxy was characterized. The thermal conductivity of epoxy is only 0.16 W m^{-1} K^{-1}. The thermal conductivity enhancement efficiency (TCE) of the filler is evaluated as

$$\mathrm{TCE} = \frac{K_c - K_p}{K_p} \quad (1)$$

where κ_c and κ_p are the thermal conductivities of nanocomposites and epoxy resin. As shown in Figure 7a, after introduction of a random three-dimensional (3D) PGO scaffold, the thermal conductivity expectedly reaches 0.81 W m^{-1} K^{-1} at 1 wt % PGO content, corresponding to 406% TCE compared with neat epoxy resin. For epoxy/random PGO (E-r-PGO) nanocomposites, the slightly high thermal conductivity mainly profits from the PGO random networks. By contrast, E-PGO shows higher thermal conductivity. The in-plane $\kappa_{//}$ (along the ice crystal growth orientation) reaches ~1.6 W m^{-1} K^{-1}, corresponding to 900% TCE compared with epoxy resin. The oriented PGO sheets connect with each other and form pathways, which decreases the thermal resistance and promotes the transmission of phonons. Compared with the E-oriented PGO (E-PGO) nanocomposite, the $\kappa_{//}$ of E-JPGO-I increases to 2.8 W m^{-1} K^{-1} and achieves 1650% TCE

https://dx.doi.org/10.1021/acsami.0c11062
ACS Appl. Mater. Interfaces 2020, 12, 44273−44280

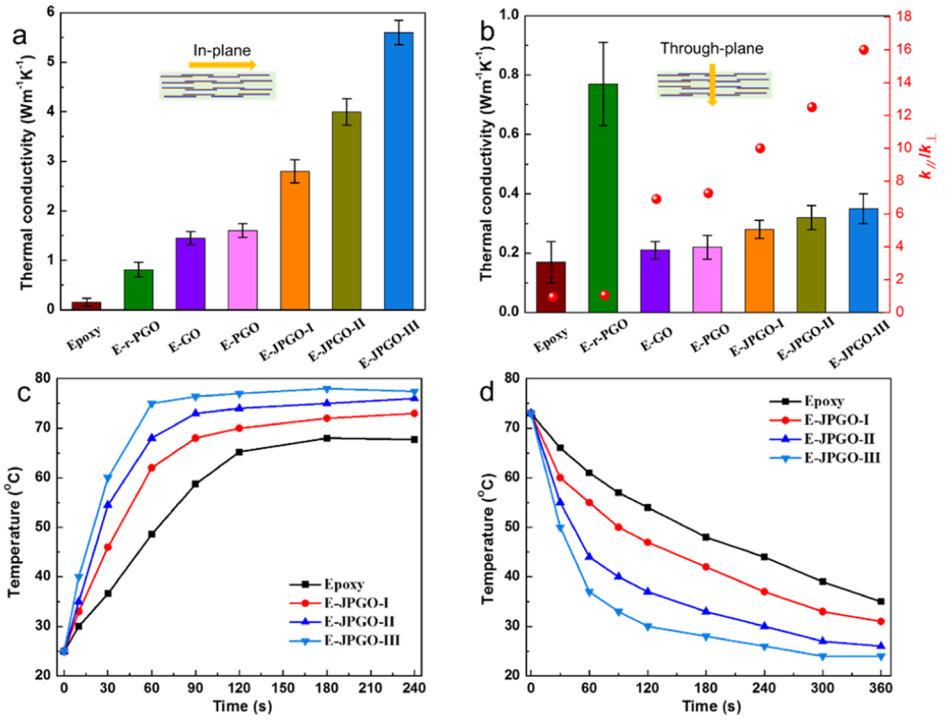

Figure 7. (a) In-plane and (b) through-plane thermal conductivity and anisotropic thermal conductivity of epoxy, E-r-PGO, E-PGO, and E-JPGO nanocomposites. (c and d) Temperature of E-JPGO nanocomposites.

compared with epoxy resin. The enhanced thermal conductive properties indicate that more thermal transfer pathways are formed. PGO owns a PDA coating on the two faces of nanosheets. Excessive PDA on the surface could induce heat flow blockage at the interface. In contrast, JPGO only has a PDA coating on the one face of nanosheets. The GO faces of JPGO in contact with each other decrease the interface thermal resistance. The JPGO scaffold structure ensures that phonons transport efficiently through GO/GO interfaces, leading to high thermal conductive properties.

By increasing the freezing rates from 5 to 20 μm s^{-1}, the layer density increases. E-JPGO-III with a higher layer density shows higher thermal conductivity than E-JPGO-I and E-JPGO-II. Quantitatively, the thermal conductivity of E-JPGO-II and E-JPGO-III was measured as 4.0, and 5.6 W m^{-1} K^{-1}, respectively. It is obvious that the interconnected JPGO nanosheets can form more heat conductive pathways with low GO/GO interfacial thermal resistance, where phonons can transfer along the JPGO scaffolds. E-JPGO nanocomposites also exhibit anisotropic thermal conduction, with through-plane ($\kappa_{\perp}$) thermal conductivities of 0.28, 0.32, and 0.35 W m^{-1} K^{-1}, respectively. The anisotropy ($\kappa_{//}/\kappa_{\perp}$) of E-JPGO nanocomposites can reach up to 16 (as shown in Figure 7b). To further demonstrate the potential application as TMMs, the heat absorption and dissipation capacities of E-JPGO nanocomposites were recorded. The nanocomposites were first placed on a heating plate at 80 °C. The temperature of E-JPGO nanocomposites exhibits a rapid increase than that of pure epoxy (Figure 7c). On the other hand, the samples were heated to 80 °C and then transferred to a steel plate (25 °C). E-JPGO nanocomposites cooled much faster than the epoxy resin (Figure 7d). These results confirm the excellent heat transfer capability of E-JPGO nanocomposites.

To demonstrate the excellence of E-JPGO nanocomposites in the thermal conductivity enhancement efficiency of polymer composites, we summarize the literature-reported thermal conductivity enhancement of polymer composites (as shown in Figure 8): E-BNNS,[24] E-PDA/CuNWs,[26] E-GO,[35] E-CEG,[36]

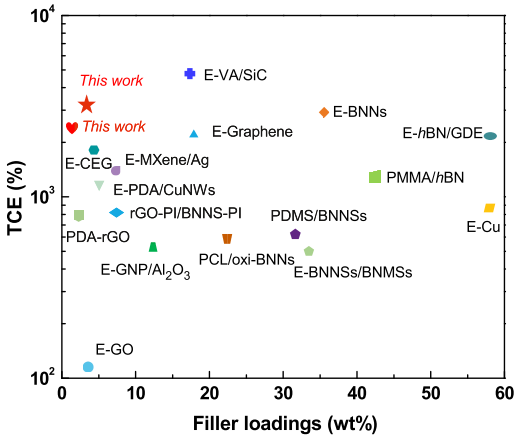

Figure 8. Comparison of the TCE between E-JPGO nanocomposites and the previously reported polymer composites.

E-Graphene,[37] E-BNNSs/BNMSs,[37] E-hBN/GDE,[38] E-MXene/Ag,[39] PDA-rGO,[40] E-VA/SiC,[41] E-Cu,[42] rGO-PI/BNNS-PI,[43] E-GNP/Al_2O_3,[44] PDMS/BNNSs,[45] PMMA/hBN,[46] and PCL/oxi-BNNs.[47] We can find that the TCE at low weight obtained in our work is the highest among these studies.

The thermal conductivity of E-JPGO-III with heating and cooling cycles was investigated. Obviously, the $k_{//}$ of E-JPGO-III shows high stability after 10 cycles (Figure 9a). As shown in Figure 9b, the electrical resistivity of epoxy is 1.91 × 10^{13} Ω cm. Obviously, the introduction of the GO scaffold decreases the volume resistivity by 7 orders of magnitude because of the

https://dx.doi.org/10.1021/acsami.0c11062
ACS Appl. Mater. Interfaces 2020, 12, 44273−44280

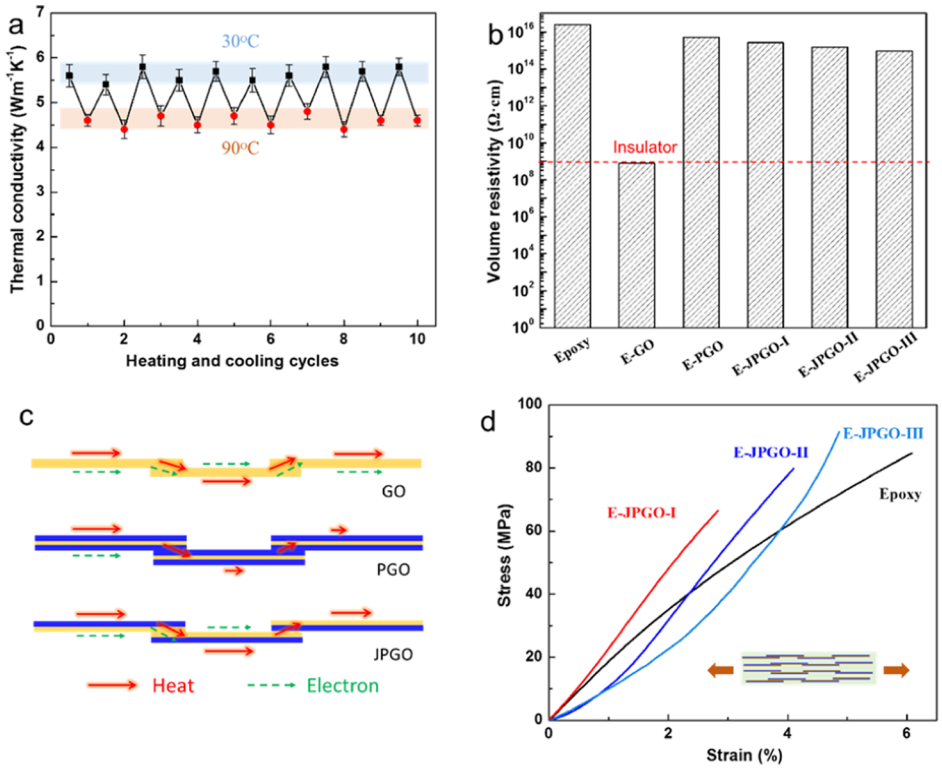

Figure 9. (a) Thermal cycling stability of E-JPGO-III. (b) Electrical resistivities of epoxy, E-GO, E-PGO, and E-JPGO nanocomposites. (c) Schematic illustration of the thermally conductive but electrically insulating mechanism in E-JPGO nanocomposites, epoxy, and E-GS nanocomposites. (d) Stress−strain curves of epoxy and E-JPGO nanocomposites.

electrically conductive path of GO sheets. However, the volume resistivities of E-PGO and E-JPGO reach 1.01×10^{14} and 5.60×10^{13} Ω cm, respectively. The PDA coating could effectively suppress the electron transport between GO sheets, thus endowing electrical insulation of nanocomposites, while the heat transfer properties of GO were preserved (Figure 9c). What is more, the volume resistivity of E-JPGO-III reaches 9.04×10^{14} Ω cm, which is far beyond the required resistance for electrical insulation (1.0×10^{9} Ω cm). The mechanical properties of E-JPGO are shown in Figure 9d. Perpendicular to the lamellar direction, the tensile strength (91.1 MPa) of E-JPGO-III is higher than that of pure epoxy (84.4 MPa). The enhancement of mechanical properties is mainly due to the interaction between JPGO and epoxy.

CONCLUSIONS

In summary, learning from nacre, we fabricated inverse artificial nacre E-JPGO nanocomposites by the bidirectional freeze-casting technique. The nanocomposites exhibit high-performance thermal conductive properties with JPGO scaffolds. Perpendicular to the lamellar structure, the thermal conductivity (in-plane) of the E-JPGO-III nanocomposite is 35 times that of pure epoxy. Furthermore, E-JPGO nanocomposites reveal excellent thermal stability and can be qualified for long-term high-temperature heat conduction applications. In addition, the nanocomposites present electrical insulating properties with a volume resistance beyond 10^{14} Ω cm due to the PDA coating on the GO surface and thus have potential applications in thermal management where graphene or metal is inapplicable.

ASSOCIATED CONTENT

Supporting Information

The Supporting Information is available free of charge at https://pubs.acs.org/doi/10.1021/acsami.0c11062.

Experiment details of preparation of graphene oxide (GO); AFM image of GO layers on the Si substrate; Raman spectra recorded at the selected GO with different number of layers; Cross section images of GO, PGO scaffolds, and epoxy nanocomposites; Cross section and side-view morphology of JPGO scaffolds (PDF)

AUTHOR INFORMATION

Corresponding Author

Weifu Dong − *The Key Laboratory of Synthetic and Biological Colloids, Ministry of Education, School of Chemical and Material Engineering, Jiangnan University, Wuxi 214122, China;* orcid.org/0000-0002-7432-8362; Phone: +86-510-8532-6290; Email: wfdong@jiangnan.edu.cn

Authors

Yang Wang − *The Key Laboratory of Synthetic and Biological Colloids, Ministry of Education, School of Chemical and Material Engineering, Jiangnan University, Wuxi 214122, China;* orcid.org/0000-0001-7875-9111

Zheng Zhang − *The Key Laboratory of Synthetic and Biological Colloids, Ministry of Education, School of Chemical and Material Engineering, Jiangnan University, Wuxi 214122, China*

Ting Li − *The Key Laboratory of Synthetic and Biological Colloids, Ministry of Education, School of Chemical and*

https://dx.doi.org/10.1021/acsami.0c11062
ACS Appl. Mater. Interfaces 2020, 12, 44273−44280

Material Engineering, Jiangnan University, Wuxi 214122, China

Piming Ma − *The Key Laboratory of Synthetic and Biological Colloids, Ministry of Education, School of Chemical and Material Engineering, Jiangnan University, Wuxi 214122, China;* orcid.org/0000-0002-4597-0639

Xuhui Zhang − *The Key Laboratory of Synthetic and Biological Colloids, Ministry of Education, School of Chemical and Material Engineering, Jiangnan University, Wuxi 214122, China*

Bihua Xia − *The Key Laboratory of Synthetic and Biological Colloids, Ministry of Education, School of Chemical and Material Engineering, Jiangnan University, Wuxi 214122, China*

Mingqing Chen − *The Key Laboratory of Synthetic and Biological Colloids, Ministry of Education, School of Chemical and Material Engineering, Jiangnan University, Wuxi 214122, China*

Mingliang Du − *The Key Laboratory of Synthetic and Biological Colloids, Ministry of Education, School of Chemical and Material Engineering, Jiangnan University, Wuxi 214122, China*

Tianxi Liu − *The Key Laboratory of Synthetic and Biological Colloids, Ministry of Education, School of Chemical and Material Engineering, Jiangnan University, Wuxi 214122, China*

Complete contact information is available at: https://pubs.acs.org/10.1021/acsami.0c11062

Notes

The authors declare no competing financial interest.

■ ACKNOWLEDGMENTS

This work was supported by the National Natural Science Foundation of China (21975108), the Natural Science Foundation of Jiangsu Province (BK20190612), MOE & SAFEA, 111 Project (B13025), the National First-Class Discipline Program of Light Industry Technology and Engineering (LITE2018-19), and the Open Research Fund Program of the Key Laboratory of Synthetic and Biological Colloids (JDSJ2018-01).

■ REFERENCES

(1) Balandin, A. A. Thermal Properties of Graphene and Nanostructured Carbon Materials. *Nat. Mater.* **2011**, *10*, 569−581.

(2) Moore, A. L.; Shi, L. Emerging Challenges and Materials for Thermal Management of Electronics. *Mater. Today* **2014**, *17*, 163−174.

(3) Bell, L. E. Cooling, Heating, Generating Power, and Recovering Waste Heat with Thermoelectric Systems. *Science* **2008**, *321*, 1457−1461.

(4) Wang, X.; Wu, P. Highly Thermally Conductive Fluorinated Graphene Films with Superior Electrical Insulation and Mechanical Flexibility. *ACS Appl. Mater. Interfaces* **2019**, *11*, 21946−21954.

(5) Chen, H.; Ginzburg, V. V.; Yang, J.; Yang, Y.; Liu, W.; Huang, Y.; Du, L.; Chen, B. Thermal Conductivity of Polymer-based Composites: Fundamentals and Applications. *Prog. Polym. Sci.* **2016**, *59*, 41−85.

(6) Wang, Y.; Xia, S.; Xiao, G.; Di, J.; Wang, J. High-Loading Boron Nitride-based Bio-inspired Paper with Plastic-like Ductility and Metal-like Thermal Conductivity. *ACS Appl. Mater. Interfaces* **2020**, *12*, 13156−13164.

(7) Cui, X.; Ding, P.; Zhuang, N.; Shi, L.; Song, N.; Tang, S. Thermal Conductive and Mechanical Properties of Polymeric Composites Based on Solution-Exfoliated Boron Nitride and Graphene Nanosheets: A Morphology-Promoted Synergistic Effect. *ACS Appl. Mater. Interfaces* **2015**, *7*, 19068−19075.

(8) Guo, S.; Zheng, R.; Jiang, J.; Yu, J.; Dai, K.; Yan, C. Enhanced Thermal Conductivity and Retained Electrical Insulation of Heat Spreader by Incorporating Alumina-Deposited Graphene Filler in Nano-Fibrillated Cellulose. *Composites, Part B* **2019**, *178*, No. 107489.

(9) He, X.; Wang, Y. Highly Thermally Conductive Polyimide Composite Films with Excellent Thermal and Electrical Insulating Properties. *Ind. Eng. Chem. Res.* **2020**, *59*, 1925−1933.

(10) Wang, Z. G.; Gong, F.; Yu, W. C.; Huang, Y. F.; Zhu, L.; Lei, J.; Xu, J. Z.; Li, Z. M. Synergetic Enhancement of Thermal Conductivity by Constructing Hybrid Conductive Network in the Segregated Polymer Composites. *Compos. Sci. Technol.* **2018**, *162*, 7−13.

(11) Pan, X.; Shen, L.; Schenning, A. P.; Bastiaansen, C. W. Transparent, High-Thermal-Conductivity Ultradrawn Polyethylene/Graphene Nanocomposite Films. *Adv. Mater.* **2019**, *31*, No. 1904348.

(12) Shtein, M.; Nadiv, R.; Buzaglo, M.; Kahil, K.; Regev, O. Thermally Conductive Graphene-Polymer Composites: Size, Percolation, and Synergy Effects. *Chem. Mater.* **2015**, *27*, 2100−2106.

(13) Ahn, C.; Kim, S.; Jung, J.; Park, J.; Kim, T.; Lee, S. E.; Jang, D.; Hong, J.; Han, S. M.; Jeon, S. Multifunctional Polymer Nanocomposites Reinforced by 3D Continuous Ceramic Nanofillers. *ACS Nano* **2018**, *12*, 9126−9133.

(14) Han, X.; Wang, T.; Owuor, P. S.; Hwang, S. H.; Wang, C.; Sha, J.; Shen, L.; Yoon, J.; Wang, W.; Salvatierra, R. V. Ultra-Stiff Graphene Foams as Three-Dimensional Conductive Fillers for Epoxy Resin. *ACS Nano* **2018**, *12*, 11219−11228.

(15) Chen, J.; Huang, X.; Sun, B.; Jiang, P. Highly Thermally Conductive Yet Electrically Insulating Polymer/Boron Nitride Nanosheets Nanocomposite Films for Improved Thermal Management Capability. *ACS Nano* **2019**, *13*, 337−345.

(16) Tian, Z.; Sun, J.; Wang, S.; Zeng, X.; Zhou, S.; Bai, S.; Zhao, N.; Wong, C. P. A Thermal Interface Material Based on Foam-Templated Three-Dimensional Hierarchical Porous Boron Nitride. *J. Mater. Chem. A* **2018**, *6*, 17540−17547.

(17) Chen, J.; Huang, X.; Zhu, Y.; Jiang, P. Cellulose Nanofiber Supported 3D Interconnected BN Nanosheets for Epoxy Nanocomposites with Ultrahigh Thermal Management Capability. *Adv. Funct. Mater.* **2017**, *27*, No. 1604754.

(18) Wu, K.; Fang, J.; Ma, J.; Huang, R.; Chai, S.; Chen, F.; Fu, Q. Achieving a Collapsible, Strong, and Highly Thermally Conductive Film Based on Oriented Functionalized Boronnbitride Nanosheets and Cellulose Nanofiber. *ACS Appl. Mater. Interfaces* **2017**, *9*, 30035−30045.

(19) Liang, Q.; Yao, X.; Wang, W.; Liu, Y.; Wong, C. A Three-Dimensional Vertically Aligned Functionalized Multilayer Graphene Architecture: An Approach for Graphene-Based Thermal Interfacial Materials. *ACS Nano* **2011**, *5*, 2392−2401.

(20) Stankovich, S.; Dikin, D. A.; Dommett, G.; Kohlhaas, K.; Zimney, E.; Stach, E. A.; Piner, R. D.; Nguyen, S. T.; Ruoff, R. S. Graphene-Based Composite Materials. *Nature* **2006**, *442*, 282−286.

(21) Shahil, K. M. F.; Balandin, A. A. Graphene−Multilayer Graphene Nanocomposites as Highly Efficient Thermal Interface Materials. *Nano Lett.* **2012**, *12*, 861−867.

(22) Peng, J.; Huang, C.; Cao, C.; Saiz, E.; Du, Y.; Dou, S.; Tomsia, A. P.; Wagner, H. D.; Jiang, L.; Cheng, Q. Inverse Nacre-Like Epoxy-Graphene Layered Nanocomposites with Integration of High Toughness and Self-Monitoring. *Matter* **2020**, *2*, 220−232.

(23) Huang, C.; Peng, J.; Wan, S.; Du, Y.; Dou, S.; Wagner, H. D.; Tomsia, A. P.; Jiang, L.; Cheng, Q. Ultra-Tough Inverse Artificial Nacre Based on Epoxy-Graphene by Freeze-Casting. *Angew. Chem., Int. Ed.* **2019**, *58*, 7636−7640.

(24) Han, J.; Du, G.; Gao, W.; Bai, H. An Anisotropically High Thermal Conductive Boron Nitride/Epoxy Composite Based on Nacre-Mimetic 3D Network. *Adv. Funct. Mater.* **2019**, *29*, No. 1900412.

(25) Liu, Y.; Ai, K.; Lu, L. Polydopamine and Its Derivative Materials: Synthesis and Promising Applications in Energy, Environmental, and Biomedical Fields. *Chem. Rev.* **2014**, *114*, 5057−5115.
(26) Yuan, H.; Wang, Y.; Li, T.; Ma, P.; Zhang, S.; Du, M.; Chen, M.; Dong, W.; Ming, W. Highly Thermal Conductive and Electrically Insulating Polymer Composites Based on Polydopamine-Coated copper Nanowire. *Compos. Sci. Technol.* **2018**, *164*, 153−159.
(27) Lian, M.; Fan, J.; Shi, Z.; Zhang, S.; Li, H.; Yin, J. Gelatin-Assisted Fabrication of Graphene-Based Nacre with High Strength, Toughness, and Electrical Conductivity. *Carbon* **2015**, *89*, 279−289.
(28) De Leon, A.; Rodier, B. J.; Luo, Q.; Hemmingsen, C. M.; Wei, P.; Abbasi, K.; Advincula, R. C.; Pentzer, E. Distinct Chemical and Physical Properties of Janus Nanosheets. *ACS Nano* **2017**, *11*, 7485−7493.
(29) Wang, Y.; Li, T.; Ma, P.; Zhang, S.; Zhang, H.; Du, M.; Xie, Y.; Chen, M.; Dong, W.; Ming, W. Artificial Nacre from Supramolecular Assembly of Graphene Oxide. *ACS Nano* **2018**, *12*, 6228−6235.
(30) Kostiuk, D.; Bodik, M.; Siffalovic, P.; Jergel, M.; Halahovets, Y.; Hodas, M.; Pelletta, M.; Pelach, M.; Hulman, M.; Spitalsky, Z. Reliable Determination of the Few-Layer Graphene Oxide Thickness Using Raman Spectroscopy. *J. Raman Spectrosc.* **2016**, *47*, 391−394.
(31) Kudin, K. N.; Ozbas, B.; Schniepp, H. C.; Prudhomme, R. K.; Aksay, I. A.; Car, R. Raman Spectra of Graphite Oxide and Functionalized Graphene Sheets. *Nano Lett.* **2008**, *8*, 36−41.
(32) Wu, N.; She, X.; Yang, D.; Wu, X.; Su, F.; Chen, Y. Synthesis of Network Reduced Graphene Oxide in Polystyrene Matrix by a Two-Step Reduction Method for Superior Conductivity of the Composite. *J. Mater. Chem.* **2012**, *22*, 17254−17261.
(33) Wang, Y.; Yuan, H.; Ma, P.; Bai, H.; Chen, M.; Dong, W.; Xie, Y.; Deshmukh, Y. S. Superior Performance of Artificial Nacre Based on Graphene Oxide Nanosheets. *ACS Appl. Mater. Interfaces* **2017**, *9*, 4215−4222.
(34) Choi, I.; Kulkarni, D. D.; Xu, W.; Tsitsilianis, C.; Tsukruk, V. V. Star Polymer Unimicelles on Graphene Oxide Flakes. *Langmuir* **2013**, *29*, 9761−9769.
(35) Huang, T.; Zeng, X.; Yao, Y.; Sun, R.; Meng, F.; Xu, J.; Wong, C. Boron Nitride@Graphene Oxide Hybrids for Epoxy Composites with Enhanced Thermal Conductivity. *RSC Adv.* **2016**, *6*, 35847−35854.
(36) Li, M.; Liu, J.; Pan, S.; Zhang, J.; Liu, Y.; Liu, J.; Lu, H. Highly Oriented Graphite Aerogel Fabricated by Confined Liquid-Phase Expansion for Anisotropically Thermally Conductive Epoxy Composites. *ACS Appl. Mater. Interfaces* **2020**, *12*, 27476−27484.
(37) Zhao, L.; Yan, L.; Wei, C.; Li, Q.; Huang, X.; Wang, Z.; Fu, M.; Ren, J. Synergistic Enhanced Thermal Conductivity of Epoxy Composites with Boron Nitride Nanosheets and Microspheres. *J. Phys. Chem. C* **2020**, *124*, 12723−12733.
(38) Lim, H.; Islam, M. A.; Hossain, M. M.; Yun, H.; Kim, M. J.; Seo, T. H.; Hahn, J. R.; Kim, B. J.; Jang, S. G. Effect of Polymeric in Situ Stabilizers on Dispersion Homogeneity of Nanofillers and Thermal Conductivity Enhancement of Composites. *Langmuir* **2020**, *36*, 5563−5570.
(39) Ji, C.; Wang, Y.; Ye, Z.; Tan, L.; Mao, D.; Zhao, W.; Zeng, X.; Yan, C.; Sun, R.; Kang, D. J.; Xu, J.; Wong, C. P. Ice-Templated MXene/Ag−Epoxy Nanocomposites as High-Performance Thermal Management Materials. *ACS Appl. Mater. Interfaces* **2020**, *12*, 24298−24307.
(40) Song, S.; Wang, J.; Liu, C.; Wang, J.; Zhang, Y. A Facile Route to Fabricate Thermally Conductive and Electrically Insulating Polymer Composites with 3D Interconnected Graphene at an Ultralow Filler Loading. *Nanoscale* **2019**, *11*, 15234−15244.
(41) Vu, M. C.; Choi, W. K.; Lee, S. G.; Park, P. J.; Kim, D. H.; Islam, M. A.; Kim, S. R. High thermal Conductivity Enhancement of Polymer Composites with Vertically Aligned Silicon Carbide Sheet Scaffolds. *ACS Appl. Mater. Interfaces* **2020**, *12*, 23388−23398.
(42) Ye, H.; Wen, H.; Chen, J.; Zhu, P.; Yuen, M. M.; Fu, X. Z.; Sun, R.; Wong, C. P. Alumina-Coated Cu@Reduced Graphene Oxide Microspheres as Enhanced Antioxidative and Electrically Insulating Fillers for Thermal Interface Materials with High Thermal Conductivity. *ACS Appl. Electron. Mater.* **2019**, *1*, 1330−1335.
(43) Guo, F.; Shen, X.; Zhou, J.; Liu, D.; Zheng, Q.; Yang, J.; Jia, B.; Lau, A. K.; Kim, J. K. Highly Thermally Conductive Dielectric Nanocomposites with Synergistic Alignments of Graphene and Boron Nitride Nanosheets. *Adv. Funct. Mater.* **2020**, *30*, No. 1910826.
(44) Sun, R.; Yao, H.; Zhang, H.-B.; Li, Y.; Mai, Y. W.; Yu, Z. Z. Decoration of Defect-Free Graphene Nanoplatelets with Alumina For Thermally Conductive and Electrically Insulating Epoxy Composites. *Compos. Sci. Technol.* **2016**, *137*, 16−23.
(45) Li, M.; Wang, M.; Hou, X.; Zhan, Z.; Wang, H.; Fu, H.; Lin, C. T.; Fu, L.; Jiang, N.; Yu, J. Highly Thermal Conductive and Electrical Insulating Polymer Composites with Boron Nitride. *Composites, Part B* **2020**, *184*, No. 107746.
(46) Morishita, T.; Okamoto, H. Facile Exfoliation and Noncovalent Superacid Functionalization of Boron Nitride Nanosheets and Their Use for Highly Thermally Conductive and Electrically Insulating Polymer Nanocomposites. *ACS Appl. Electron. Mater.* **2016**, *8*, 27064−27073.
(47) Lee, J.; Jung, H.; Yu, S.; Cho, S. M.; Tiwari, V. K.; Velusamy, D. B.; Park, C. Boron Nitride Nanosheets (BNNSs) Chemically Modified by "Grafting-From" Polymerization of Poly(caprolactone) for Thermally Conductive Polymer Composites. *Chem. - Asian J.* **2016**, *11*, 1921−1928.

https://dx.doi.org/10.1021/acsami.0c11062
ACS Appl. Mater. Interfaces 2020, 12, 44273−44280